Theoretical investigation of the photon efficiency in frequency-domain fluorescence lifetime imaging microscopy

Alan Elder, Simon Schlachter, and Clemens F. Kaminski*

Department of Chemical Engineering, University of Cambridge, Pembroke Street, Cambridge, UK
**Corresponding author: cfk23@cam.ac.uk*

Received July 6, 2007; revised November 18, 2007; accepted December 11, 2007;
posted December 17, 2007 (Doc. ID 84840); published January 29, 2008

We investigate the photon efficiency of frequency-domain fluorescence lifetime imaging microscopy, using both theoretical and Monte Carlo methods. Our analysis differs from previous work in that it incorporates the data fitting process used in real experiments, allows for the arbitrary choice of excitation and gain waveforms, and calculates lifetimes as well as associated *F*-values from higher harmonics in the data. Using our analysis, we found different photon efficiencies to those previously reported and were able to propose optimal excitation and gain waveforms. Additionally, we suggest measurement protocols that lead to further improvement in photon efficiency. We compare our results to other techniques for lifetime imaging and consider the implications of our higher-harmonic analysis for multi-exponential lifetime determination. © 2008 Optical Society of America

OCIS codes: 000.5490, 170.2520, 170.3650, 180.2520.

1. INTRODUCTION

Fluorescence microscopy is extensively used in many research areas, particularly in the biological sciences. The emission properties of a fluorophore reflect the local molecular environment in which it resides. Changes in, for example, pH, ion concentration, viscosity, temperature, proximity to other fluorophores, and the presence of quenchers can all affect the properties of the observed fluorescence, including changes in intensity, lifetime, polarization, and wavelength. One powerful method commonly used in this context is fluorescence lifetime imaging microscopy (FLIM) [1]. FLIM provides information on photophysical events that cannot be measured with simple intensity measurements [2].

Several different FLIM systems are now commercially available, operating in both the time domain and in the frequency domain. Time-domain techniques rely on using a pulsed excitation source followed by measurement of the emission as a function of time. For point scanning devices, time-correlated single-photon counting (TCSPC) is commonly used, where the arrival times of individual photons following each excitation pulse are recorded [3,4]. For widefield microscopy, time-gated imaging has been employed, in which a gated image intensifier is used to measure the integrated fluorescence in consecutive time windows following each excitation pulse [5]. In frequency-domain FLIM (FD-FLIM) the excitation is temporally modulated and the lifetime can be determined by measuring the phase shift or demodulation of the detected fluorescence signal relative to the excitation signal. For widefield microscopy a homodyne detection scheme is used to determine the phase shift and demodulation, where the detector gain is modulated at the same frequency as the excitation and images are taken at a series of relative phase offsets. By fitting a sinusoid to the modulated signals, the phase shift and demodulation of the fluorescence emission can be recovered. For detection, a multichannel plate (MCP) intensified CCD is often used with the gain modulated by modulating the photocathode voltage [6,7].

The relative efficiency of these different methods for lifetime determination is an important differentiating factor. One way of estimating the accuracy is by using the so called *F*-value [8]. The *F*-value is described as the "normalized relative RMS noise" and is calculated using Eq. (1), where τ is the lifetime, σ_τ is the standard deviation of the lifetime, and N is the total number of photons. Here σ_τ/τ is the relative RMS noise of the lifetime measurement, which is normalized by the relative RMS noise of the shot-noise-limited intensity measurement, $\sqrt{N}/N$.

$$F = \frac{\sqrt{N}\sigma_\tau}{\tau}. \tag{1}$$

The optimal theoretically achievable *F*-value is 1. Higher *F*-values indicate poorer performance. The *F*-value squared represents the relative number of photons required for a given measurement accuracy compared to the shot-noise limit. The *F*-value is hence a valuable tool for comparing the performance of different imaging techniques or different modes of operation within the same technique.

The *F*-value has been investigated in the literature for time-domain methods [9–11] and frequency-domain methods [12,13]. With TCSPC, *F*-values very close to 1.0 are obtained [11]. For time-gated systems with parallel acquisition, the best achievable *F*-value depends on the number of gates used. Two-, four-, and eight-gate configurations have been found to have minimum *F*-values of 1.7, 1.3, and 1.23, respectively [9]. In the frequency-domain work, different excitation and gain waveforms were inves-

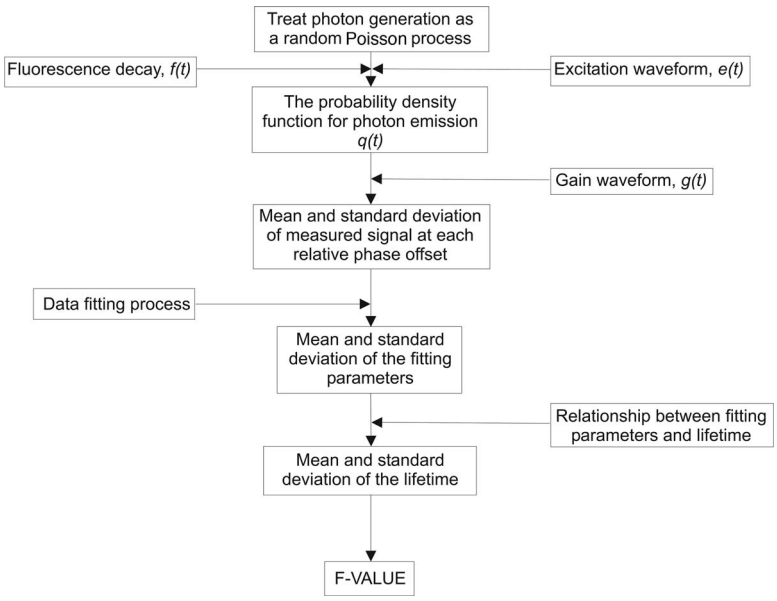

Fig. 1. Schematic showing the processes involved in calculating an F-value for FD-FLIM.

tigated for both the case of lock-in detection and homodyne detection using an image intensifier. Better F-values were obtained for lock-in detection, though this is still a developing technology for widefield microscopy measurements [14], and so we consider only the image intensifier case. Using an image intensifier the best reported F-value was 7.4 for sinusoidal excitation with sinusoidal gain, and 2.1 for Dirac excitation with sinusoidal gain [12].

The excellent paper by Phillip and Carlsson [12] provides a good insight into the F-values obtainable with FD-FLIM. However, we see an opportunity to extend their work in several ways. First, the method with which F-values for FD-FLIM were calculated in [12] does not fully reflect the experimental protocol that is commonly used today. In actuality, the homodyne detection scheme is realized by taking measurements at a series of different phase shifts between excitation and gain waveforms, typically between 6 and 12 [6]. A sinusoid is fitted to this data, from which the lifetime can then be extracted. In [12] the data fitting procedure was simplified by taking two measurements at different phase angles and a third measurement with the modulation switched off. Second, the ability of FD-FLIM to analyze lifetimes from higher harmonics in the data was not assessed. Finally, the excitation and gain profiles could not be varied arbitrarily (modulation depth, harmonic content, etc.).

In this work we develop a general statistical framework for calculation of F-values for FD-FLIM with an image intensifier that incorporates the commonly used data fitting process. By expressing the waveforms as a Fourier series, the method allows for the choice of arbitrary gain and excitation waveforms with an arbitrary number of phase steps. It also allows the investigation of lifetimes evaluated from higher-harmonic components. Monte Carlo simulations were performed in order to back up the theoretical findings. The results show that F-values achievable with FD-FLIM depend heavily on the imaging parameters used. Based on the findings, we suggest optimal excitation and gain waveforms, as well as innovative experimental and data fitting procedures that further improve the fidelity of FD-FLIM measurements, and consider the potential of higher-harmonic lifetime analysis.

2. OVERVIEW OF THEORETICAL CALCULATIONS

We begin by treating photon generation as a random Poissonian process. Combined with knowledge of the excitation waveform and assuming a single-exponential fluorescence decay, the probability density function (PDF) for photon emission as a function of time, $q(t)$, can be calculated. Knowledge of the PDF and the detection waveform can then be used to find the expected value and standard deviation of the measured signal for each relative phase offset. By knowing the way in which the data fitting process combines the signals from each relative phase offset measurement, the expected value and standard deviation of each of the fitting parameters can be found. Finally, by using the relationship between phase or modulation lifetimes and the fitted parameters, the expected value and standard deviation of either the phase or modulation lifetime can be calculated. This process is demonstrated schematically in Fig. 1.

Once the expectation and standard deviation of the lifetime have been calculated, we can work out the F-value using Eq. (1). Calculations are performed for both Dirac excitation and multiharmonic sinusoidal excitation with a multiharmonic sinusoidal gain waveform. Using Fourier series allows us to express any arbitrary excitation waveform.

3. FLUORESCENCE MODEL

In order to make calculations easier, we adopt dimensionless variables, as introduced by Philip and Carlsson [12]:

$$t = \frac{2\pi}{T}t^*, \qquad \tau = \frac{2\pi}{T}\tau^*, \tag{2}$$

where t^* is time in seconds, τ^* is the fluorescence lifetime in seconds, and T is the time period of the illuminating light; T is related to the angular frequency of the illuminating light, ω, by the relationship $T=2\pi/\omega$.

Using this notation, we describe the fluorescence caused by a Dirac light pulse at time $t=0$ as

$$f(t) = \frac{1}{\tau}\exp\left(-\frac{t}{\tau}\right), \qquad t \geqslant 0, \tag{3}$$

where $f(t)$ is normalized so that its integral over time greater than zero is equal to one.

When we excite with modulated illumination, the fluorescence observed will be a convolution between the illumination waveform, $e(t)$, and the fluorescence response to a delta function, $f(t)$. Because the fluorescence light is weak, we can think of it as a series of photons rather than a continuous flow. The convolution $e(t)\otimes f(t)$ will then be proportional to the PDF for photon emission, which will form the basis of our analysis.

4. PHOTON EMISSION PROBABILITY DENSITY FUNCTION, $q(t)$

A. Multiharmonic Sinusoidal Excitation

The excitation signal is described by a sum of sine waves

$$e(t) = \frac{1 + \sum_{j=1}^{J} m_{ex,j}\sin(jt)}{2\pi}, \tag{4}$$

where j represents the harmonic, J represents the total number of harmonics, and $m_{ex,j}$ represents the modulation depth of the jth harmonic.

Taking the convolution of $e(t)$ and $f(t)$ and rearranging using standard trigonometric identities gives the photon PDF, $q(t)$,

$$2\pi q(t) = 1 + \sum_{j=1}^{J} \frac{m_{ex,j}}{(1+(j\tau)^2)^{1/2}}(\sin(jt-\alpha_j)),$$

where

$$\alpha_j = \arctan(j\tau). \tag{5}$$

In order to make the handling of the periodic functions easier, we define the Fourier coefficients of $q(t)$ as

$$q_k = \int_0^{2\pi} \exp(-ikt)q(t)\mathrm{d}t.$$

We find

$$q_k = \left.\begin{array}{l} 1 \end{array}\right\} \quad k = 0, \tag{6}$$

$$q_k = \frac{m_{ex,|k|}}{(1+(k\tau)^2)}\left(\frac{-k}{|k|}\right)\left(\frac{i+k\tau}{2}\right) \quad \left.\begin{array}{l} \\ \end{array}\right\} \quad k \neq 0. \tag{7}$$

B. Dirac Excitation

The excitation signal is now described as a series of delta functions. We find the PDF for this case to be

$$q(t) = \frac{\exp(-t/\tau)}{\tau(1-\exp(-2\pi/\tau))}, \qquad 0 \leqslant t < 2\pi.$$

Note that the expression is normalized so that the integral of $q(t)$ over one period is equal to 1.

The Fourier coefficients are then given by

$$q_k = \frac{1}{1+ik\tau}. \tag{8}$$

5. HOMODYNE DETECTION SCHEME

We wish to find the expectation and standard deviation of the fluorescence signal at phase step i, corresponding to a phase offset of ϕ_i^g. We start by letting X_i be a random variable describing the fluorescence signal from a single excitation photon at phase step i. It follows that for a measurement with N_p excitation photons per phase step, the fluorescence signal at phase step i will have a mean of $N_pE(X_i)$ and a variance of $N_p\sigma_{X_i}^2$. The measured fluorescence signal, y_i, will be an estimate of N_pX_i.

For a periodic function, $g(t)$, with probability density $p(t)$, the expectation of that function can be written as

$$E(g(t)) = \int_0^{2\pi} g(t)p(t)\mathrm{d}t.$$

Let us describe the gain of the intensifier as $g(t)=a+\Sigma_{j=1}^{J}b_j\sin(j(t-\phi_i^g))$. Here J is the number of harmonics to be considered in the analysis. Then $E(X_i)$ is given by

$$E(X_i) = \int_0^{2\pi}\left(a + \sum_{j=1}^{J} b_j\sin(j(t-\phi_i^g))\right)q(t)\mathrm{d}t. \tag{9}$$

A. Calculation of $E(X_i)$

Using Eq. (9), $E(X_i)$ can be calculated for either the case of Dirac or multiharmonic sinusoidal excitation simply by inserting the correct form of the PDF, as calculated in Section 4.

For multiharmonic sinusoidal excitation, using Eqs. (6) and (7) for q_k, we find

$$E(X_i) = a + \sum_{j=1}^{J}\left(\frac{b_jm_{ex,j}}{2(1+(j\tau)^2)^{1/2}}\right)\cos(j\phi_i^g - \alpha_j). \tag{10}$$

For Dirac excitation the calculation is similar except q_k is given by Eq. (8). We obtain

$$E(X_i) = a + \sum_{j=1}^{J}\frac{b_j\cos(j\phi_i^g - \xi_j)}{(1+(j\tau)^2)^{1/2}}, \tag{11}$$

where

$$\xi_j = \arctan\left(-\frac{1}{j\tau}\right). \tag{12}$$

B. Calculation of $\sigma^2_{X_i}$

The standard deviation of X_i is equal to $E(X_i^2)$, as described in the work by Philip and Carlsson [12]. Here $E(X_i^2)$ is given by

$$E(X_i^2) = \int_0^{2\pi} \left(a + \sum_{j=1}^{J} b_j \sin(j(t - \phi_i^g)) \right)^2 q(t) \mathrm{d}t. \quad (13)$$

For multiharmonic sinusoidal excitation we find

$$E(X_i^2) = q_0 a^2 + 2a \sum_{j=1}^{J} \left(\frac{b_j m_{ex,j}}{2(1+(j\tau)^2)^{1/2}} \right) \cos(j\phi_i^g - \alpha_j) \cdots + \cdots \sum_{j=1}^{J} \sum_{k=1}^{J} \frac{b_j b_k}{2} \Re[\exp(-(j-k)\phi_i^g i) q_{(k-j)} \cdots \cdots - \exp(-(j+k)\phi_i^g i) q_{-(j+k)}].$$

Using the expressions for q_k [Eqs. (6) and (7)] gives $E(X_i^2)$.

For Dirac excitation a similar analysis is used, but with q_k given by Eq. (8).

6. DATA FITTING PROCESS

In order to obtain lifetime information, FD-FLIM measurements are taken at a series of different relative phase offsets between the illumination and the gain waveforms. The signal as a function of relative phase shift is periodic, as can be seen from Eqs. (10) and (11). Lifetime information is extracted by fitting a series of sinusoids to this data and determining the phase shift and demodulation. Because we wish to analyze lifetimes from several harmonic components of the signal, we fit a function of the form

$$y_i = a_1 + \sum_{j=1}^{H} \alpha_2^j \cos(j\phi_i^g - \alpha_3^j). \quad (14)$$

The modulation and phase shift for the jth harmonic component are then given respectively by

$$\phi_{spl}^j = \alpha_3^j, \qquad m_{spl}^j = \frac{\alpha_2^j}{a_1}. \quad (15)$$

Since we need to fit to data in a large number of pixels, an efficient fitting algorithm is required. This can be achieved by linearizing Eq. (14), such that only a matrix multiplication is required to perform the fitting in each pixel. An alternative to this is to use a Fourier sine estimator, which involves taking the Fourier transform of the data [15]. The Fourier estimator works only in the case of equidistant phase shifts over a 2 π range and is in this case identical to the linearized sine estimator [16]. We choose to use the linearized sine estimator approach, as it makes visualization of the fitting process clearer and also allows uneven phase steps to be analyzed.

A. Linear Least-Squares Fitting Procedure

We write our fitting function as a linear function in the variables $x_i^{1,j} = \cos(j\phi_i^g)$ and $x_i^{2,j} = \sin(j\phi_i^g)$ by expanding the cosine term in Eq. (14). Defining the parameters $\theta_1 = a_1$, $\theta_2^j = \alpha_2^j \cos(\alpha_3^j)$, and $\theta_3^j = \alpha_2^j \sin(\alpha_3^j)$, the linearized fitting function can be written as

$$y_i = \theta_1 + \sum_{j=1}^{H} (\theta_2^j x_i^{1,j} + \theta_3^j x_i^{2,j}). \quad (16)$$

The least-squares estimate of the fitting parameters, $\underline{\theta}_{LS}$, is given by [17]

$$\underline{\theta}_{LS} = [(\mathbf{X}^T\mathbf{X})^{-1}\mathbf{X}^T]\underline{y}, \quad (17)$$

where

$$\mathbf{X} = \begin{pmatrix} \cdots & \underline{x}_1 & \cdots \\ \cdots & \underline{x}_2 & \cdots \\ & \vdots & \\ \cdots & \underline{x}_N & \cdots \end{pmatrix}, \qquad \underline{x}_i = (1 \quad x_i^{1,1} \quad x_i^{2,1} \quad \cdots \quad x_i^{1,H} \quad x_i^{2,H}).$$

The matrix $\mathbf{X}$ depends only on the phase steps used and the number of harmonics fitted. For the case of evenly spaced phase steps the calculation is simplified, as $(\mathbf{X}^T\mathbf{X})^{-1}$ is diagonal, and the least-squares estimate of the fitting parameters is given by

$$\underline{\theta}_{LS} = \begin{pmatrix} \theta_1 \\ \theta_2^1 \\ \theta_3^1 \\ \vdots \\ \theta_2^H \\ \theta_3^H \end{pmatrix} = \begin{pmatrix} \frac{1}{N}\sum_{i=1}^{N} y_i \\ \frac{2}{N}\sum_{i=1}^{N} y_i \cos(\phi_i^g) \\ \frac{2}{N}\sum_{i=1}^{N} y_i \sin(\phi_i^g) \\ \vdots \\ \frac{2}{N}\sum_{i=1}^{N} y_i \cos(H\phi_i^g) \\ \frac{2}{N}\sum_{i=1}^{N} y_i \sin(H\phi_i^g) \end{pmatrix}. \quad (18)$$

We present the following analysis based on the assumption of evenly spaced phase steps. If the phase steps are not even, then calculation of $\mathbf{X}$ is still straightforward, but $(\mathbf{X}^T\mathbf{X})^{-1}$ will no longer be diagonal. The least-squares estimate of each fitting parameter will still be a linear combination of the experimental measures, y_i, and so the analysis methodology presented is still valid.

B. Expectation and Standard Deviation of Fitting Parameters

To estimate the accuracy of the fitting parameters, we let U^j, V^j, and W be random variables with the respective means μ_u^j, μ_v^j, and μ_w and standard deviations σ_u^j, σ_v^j, and σ_w, which are equivalent to the parameters θ_3^j, θ_2^j, and θ_1, respectively. Since y_i is an estimate of $N_p X_i$, from Eq. (18) we can write U^j, V^j, and W as

$$U^j = \frac{2}{N}\sum_{i=1}^{N} N_p X_i \sin(j\phi_i^g),$$

$$V^j = \frac{2}{N}\sum_{i=1}^{N} N_p X_i \cos(j\phi_i^g),$$

$$W = \frac{1}{N}\sum_{i=1}^{N} N_p X_i. \tag{19}$$

For convenience we write N_pX_i as $N_pX_i = \mu_i + \sigma_i Y_i$, where μ_i is the mean and σ_i is the standard deviation of the fluorescence signal for N_p excitation photons in phase step i; Y_i is a random variable with mean 0 and variance 1. Here i can be any integer from 1 to N and indicates the phase step number, and μ_i and σ_i are related to the already calculated $E(X_i)$ and $E(X_i^2)$ by the following equations:

$$\mu_i = N_p E(X_i), \qquad \sigma_i^2 = N_p E(X_i^2), \tag{20}$$

as described in Section 5.

Taking the expectation of Eq. (19), we can calculate $E(U^j)$ as

$$E(U^j) = \frac{2}{N}\sum_{i=1}^{N} [\mu_i \sin(j\phi_i^g) + E(\sigma_i Y_i \sin(j\phi_i^g))].$$

Since $E(Y_i)=0$,

$$E(U^j) = \frac{2}{N}\sum_{i=1}^{N} \mu_i \sin(j\phi_i^g). \tag{21}$$

A similar analysis gives V^j and W.

The standard deviation of U^j is calculated by first determining $E(U^{j^2})$. The standard deviation is then calculated from $\sigma_{U^j}^2 = E(U^{j^2}) - E(U^j)^2$.

Squaring Eq. (19) and then taking expectations yields

$$E(U^{j^2}) = \frac{4}{N^2} E\left(\sum_{i=1}^{N}\sum_{k=1}^{N} (\mu_i\mu_k + \mu_i\sigma_k Y_k + \mu_k\sigma_i Y_i + \sigma_i\sigma_k Y_i Y_k)\sin(j\phi_i^g)\sin(j\phi_i^g)\right).$$

Now, since measurements in phase steps i and k ($i,k = 1\ldots N$) are independent, $E(Y_iY_k) = E(Y_i)E(Y_k) = 0$. Also $E(Y_i^2) = 1$ and $E(Y_i) = 0$, which gives

$$E(U^{j^2}) = E(U^j)^2 + \frac{4}{N^2}\sum_{i=1}^{N} (\sigma_i^2)\sin^2(j\phi_i^g). \tag{22}$$

$E(V^{j^2})$, $E(W^2)$, $E(U^jV^j)$, $E(U^jW)$, and $E(V^jW)$ are found in the same way. Because $E(X_i)$ and $E(X_i^2)$ were already calculated in Section 5, μ_i and σ_i can be calculated from Eq. (20).

7. LIFETIME ANALYSIS

A. Relationship between Lifetime and Fitting Parameters for Multiharmonic Sinusoidal Excitation

The phase lifetime is calculated from the phase shift in the detected signal. On inspection of Eq. (10), we see that

$$j\tau_p^j = \tan(\phi_{spl}^j).$$

Including the definitions of the fitting parameters, we find

$$j\tau_p^j = \frac{\theta_3^j}{\theta_2^j}. \tag{23}$$

The modulation lifetime is calculated from the demodulation in the detected signal. From Eq. (10) we see that

$$\tau_m^j = \left(\left(\frac{m_{gain}^j m_{ex}^j}{2m_{spl}^j}\right)^2 - 1\right)^{1/2}.$$

Including the definitions of the fitting parameters, we find

$$j\tau_m^j = \left(\left(\frac{\theta_1{}^2 m_{gain}^j{}^2 m_{ex}^j{}^2}{4(\theta_2^j{}^2 + \theta_3^j{}^2)}\right) - 1\right)^{1/2}. \tag{24}$$

B. Relationship between Lifetime and Fitting Parameters for Dirac Excitation

For Dirac excitation a similar analysis yields

$$-\frac{1}{j\tau_p^j} = \frac{\theta_3^j}{\theta_2^j}, \tag{25}$$

$$j\tau_m^j = \left(\left(\frac{\theta_1{}^2 m_{gain}^j{}^2}{\theta_2^j{}^2 + \theta_3^j{}^2}\right) - 1\right)^{1/2}. \tag{26}$$

C. Expectation and Standard Deviation of Lifetimes for Multiharmonic Sinusoidal Excitation

Using the random variables U^j and V^j introduced in Section 6 and writing $U^j = \mu_U^j + \sigma_U^j Y_U^j$ and $V^j = \mu_V^j + \sigma_V^j Y_V^j$, the scaled phase lifetime, τ_p^j, can be written as

$$j\tau_p^j = \frac{U^j}{V^j} = \frac{\mu_u^j + \sigma_u^j Y_u^j}{\mu_v^j + \sigma_v^j Y_v^j},$$

where μ_U^j and μ_V^j are the means, σ_U^j and σ_V^j are the standard deviations, and Y_U^j and Y_V^j are random variables with mean zero and variance equal to one for harmonic j.

By calculating $E(\tau_p^j)$ and $E(\tau_p^j{}^2)$, we are able to calculate both the mean and the standard deviation in the expected value of τ_p^j from $\sigma_{\tau_p^j}^2 = E(\tau_p^{j^2}) - E(\tau_p^j)^2$. In order to do this, we introduce the notation $\kappa_u^j = \sigma_u^j/\mu_u^j$ and $\kappa_v^j = \sigma_v^j/\mu_v^j$. Assuming that κ_u^j is much less than unity and using a series expansion, we find

$$\frac{U^j}{V^j} = \frac{\mu_u^j}{\mu_v^j}(1 + \kappa_u^j Y_u^j - \kappa_v^j Y_v^j - \kappa_u^j\kappa_v^j Y_u^j Y_v^j + \kappa_v^j{}^2 Y_v^j{}^2 + \cdots).$$

Putting this expression into Eq. (23) and using the fact that $E(Y_u^j) = 0$, $E(Y_v^j) = 0$, and $E(Y_v^j{}^2) = 1$ gives

$$E(\tau_p^j) = \frac{1}{j}\frac{\mu_u^j}{\mu_v^j}(1 - \rho_{uv}^j\kappa_u^j\kappa_v^j + \kappa_v^{j\,2} + \cdots), \tag{27}$$

where $\rho_{uv}^j = E(Y_u^j Y_v^j) = [E(U^j V^j) - E(U^j)E(V^j)]/\sigma_U^j\sigma_V^j$.

Squaring the expression for U^j/V^j and ignoring terms of order greater than 2, we obtain an expression for the expectation of τ_p^j squared, $E(\tau_p^{j2})$, and hence find the standard deviation of τ_p^j.

For the modulation lifetime we take a similar approach. Writing $W = \mu_W + \sigma_W Y_W$, and with reference to Eq. (24), the scaled modulation lifetime τ_m^j can be written as

$$j\tau_m^j = \left(\frac{(\mu_w + \sigma_w Y_w)^2 - z^j(\mu_u^j + \sigma_u^j Y_u^j)^2 - z^j(\mu_v^j + \sigma_v^j Y_v^j)^2}{z^j(\mu_u^j + \sigma_u^j Y_u^j)^2 + z^j(\mu_v^j + \sigma_v^j Y_v^j)^2}\right)^{1/2}.$$

Here z^j is a constant defined by the equation

$$z^j = \frac{4}{m_{ex}^{j\,2} m_{gain}^{j\,2}}. \tag{28}$$

As for the phase lifetime case, we wish to calculate $E(\tau_m^j)$ and $E(\tau_m^{j2})$. In order to do this, we introduce the notation

$$\beta_k^{j2} = \left(\frac{\sigma_k^{j2}}{\mu_w^2 - z^j\mu_u^{j2} - z^j\mu_v^{j2}}\right), \tag{29}$$

$$\gamma_k^j = \left(\frac{2\mu_k^j\sigma_k^j}{\mu_w^2 - z^j\mu_u^{j2} - z^j\mu_v^{j2}}\right), \tag{30}$$

$$\delta_k^{j2} = \left(\frac{\sigma_k^{j2}}{\mu_u^{j2} + \mu_v^{j2}}\right), \tag{31}$$

$$\epsilon_k^j = \left(\frac{2\mu_k^j\sigma_k^j}{\mu_u^{j2} + \mu_v^{j2}}\right), \tag{32}$$

where k can be u, v, or w.

Assuming β_k^j, γ_k^j, δ_k^j, and ϵ_k^j to be small so that terms of order 3 and higher can be ignored and using series expansions allows $E(\tau_m^j)$ to be calculated in a way similar to $E(\tau_p^j)$.

A similar analysis is performed to calculate $E(\tau_m^{j\,2})$ to obtain the variance of τ_m^j as in the phase lifetime case.

D. Expectation and Standard Deviation of Lifetimes for Dirac Excitation

The calculations for Dirac excitation are very similar to the ones for multiharmonic sinusoidal excitation but start with Eqs. (25) and (26).

8. *F*-VALUE CALCULATION

For the measurement scheme presented here we define the *F*-value as in Eq. (33):

$$F = \frac{\sqrt{NN_p}\sigma_\tau}{\tau}. \tag{33}$$

Here the term NN_p represents the total number of photons used in the measurement (the number of phase steps multiplied by the number of photons per phase step measurement). A program was written in IDL (Interactive Data Language, Research Systems, Inc.) in order to use the analytical expressions developed in this paper to calculate the *F*-value for a wide range of different scenarios. The results of these calculations are presented below.

9. MONTE CARLO SIMULATIONS

In order to back up the calculations presented in this paper, Monte Carlo simulations of the FD-FLIM measurements were also performed. The Monte Carlo simulations performed were similar to those described by [13]. A flow diagram explaining the main steps of the Monte Carlo simulation is shown in Fig. 2. For each Monte Carlo experiment the number of axis divisions, M, was chosen as 1000 in order to keep the probability $q(t)\Delta t$ below $\sim$0.01 and hence reduce the chance of several photons occurring per interval; N_p was taken as 2500. Varying M or N_p around these values was found to have a negligible influence on the results. Each simulation was repeated 500 times in order to produce reliable statistics.

In all cases, results from the Monte Carlo simulations agreed well with the theoretical calculations, as presented in the Results.

10. RESULTS

For $N \geqslant 4$ we found that changing the number of phase steps had very little impact on the calculated *F*-values. We also found that shifting the phase of evenly distributed phase steps had no impact on the *F*-values. As such, all results for $N \geqslant 4$ are general results for evenly distributed phase steps.

When evenly spaced phase steps are used and the Nyquist sampling criterion is satisfied, the matrix $\mathbf{X}^T\mathbf{X}^{-1}$ is diagonal, and so fitting higher harmonics does not affect the fit of lower harmonics. When uneven phase steps are used, this is no longer true, and if higher harmonics present in the signal are not accounted for, then there can be artifacts in the data due to aliasing. As such, the data presented here use evenly spaced phase steps except where explicitly stated.

A. Sinusoidal Gain, $N \geqslant 4$

For sinusoidal excitation and sinusoidal gain with modulation depths of 1 (see Fig. 3), we found an optimum phase *F*-value of 9.0 at $\tau = 0.7$ and an optimum modulation *F*-value of 8.7 at $\tau = 1.35$. Further testing showed that decreasing the modulation depth of either the excitation or gain waveform led to significantly poorer *F*-values (decreasing the excitation modulation depth to 0.5 increased the minimum phase and modulation *F*-values to 18.0 and 17.8, respectively, while the same for the gain modulation depth led to values of 15.6 and 15.4, respectively).

For Dirac excitation and sinusoidal gain with a modulation depth of 1 (see Fig. 4), we found an optimum phase *F*-value of 4.28 for $\tau = 0.68$ and an optimum modulation *F*-value of 3.9 at $\tau = 1.18$. Decreasing the modulation

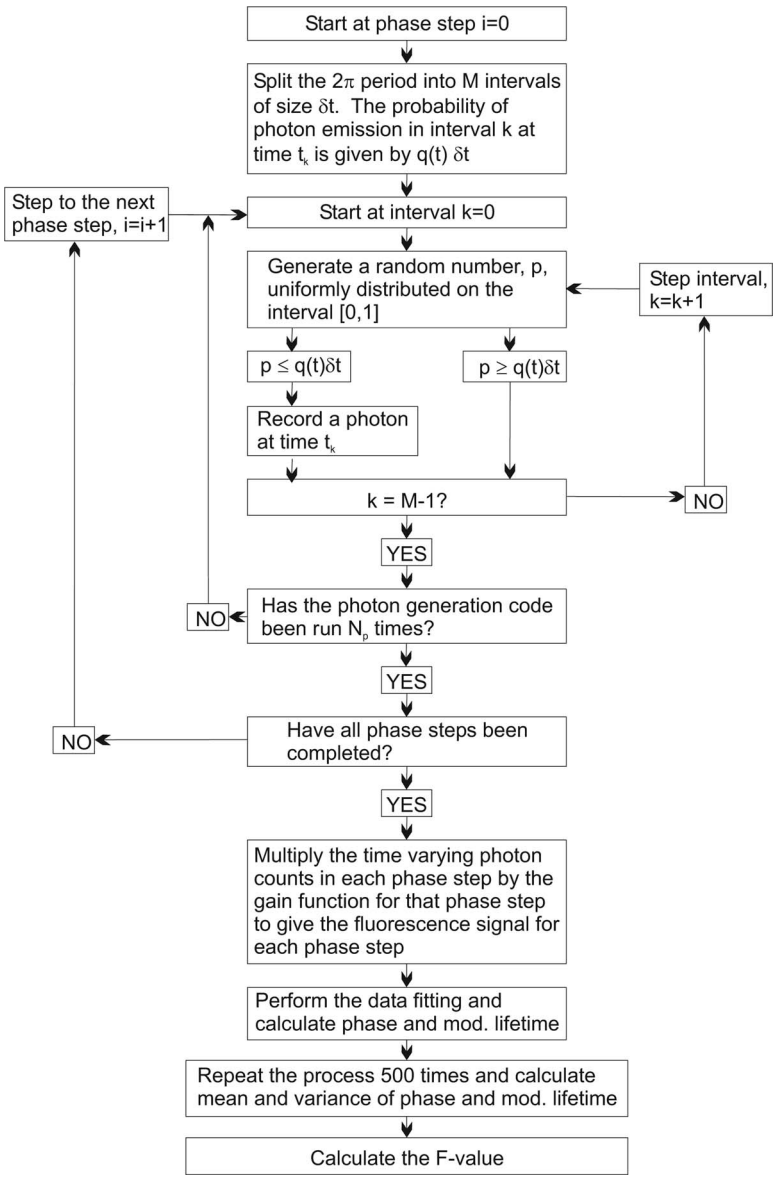

Fig. 2. Flow diagram showing the process followed by the Monte Carlo simulations.

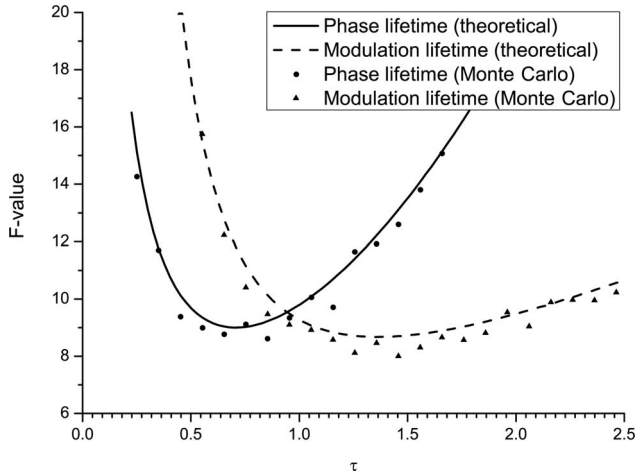

Fig. 3. Graph showing the *F*-value as a function of τ for sinusoidal excitation (modulation depth of 1.0) with sinusoidal gain (modulation depth of 1.0) for phase and modulation lifetimes. Both the theoretical results and Monte Carlo simulation data are shown, which are in good agreement.

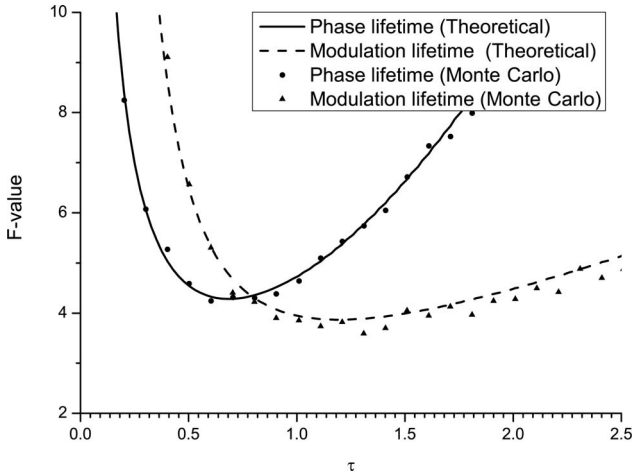

Fig. 4. Graph showing the *F*-value as a function of τ for Dirac excitation with sinusoidal gain (modulation depth of 1.0) for phase and modulation lifetimes. Both the theoretical and Monte Carlo simulation data sets are shown, and the agreement is excellent.

depth of the gain had a detrimental effect on the F-values similar to that for the sinusoidal excitation case.

B. Sinusoidal Gain, $N=3$

For $N=3$ we found F-values for the case of sinusoidal gain different from those for $N \geqslant 4$. We also found that shifting the locations of three evenly distributed phase steps caused the F-value to change. We found optimum F-values of 7.6 ($\tau=0.68$, $\phi^g=[35°,155°,275°]$) and 7.8 ($\tau=1.31$, $\phi^g=[-5°,115°,235°]$) for phase and modulation lifetimes, respectively. The phase lifetime calculation is an analogous case to the calculation for an image intensifier in [12], where a value of 7.4 at $\tau=0.69$ was found.

With Dirac excitation, similar results were found, with optimal phase and modulation F-values of 2.6 ($\tau=0.58$, $\phi^g=[61°,181°,301°]$) and 2.4 ($\tau=0.65$, $\phi^g=[5°,125°,245°]$), respectively. These data are shown in Fig. 5.

C. Multiharmonic Analysis

By using a Fourier series representation, we can use any function for either the gain or excitation waveform. This allows us to evaluate lifetimes and corresponding F-values for each higher harmonic present in both excitation and gain waveforms.

To avoid aliasing problems, we found that using $N>J+H$ lead to accurate lifetime estimates without aliasing problems. For analysis of a square wave we used the first 13 terms of the Fourier series representation and attempted to fit harmonics 1, 3, and 5. Hence >18 phase steps were used. Using more phase steps had no impact on the F-values, as was the case with sinusoidal gain.

For multiharmonic sinusoidal excitation, we found that adding extra harmonics to either the excitation or gain waveform had very little effect on the F-values calculated from the other harmonics (for either phase or modulation lifetime). The important factor was the gain and excitation modulation depth of the harmonic of interest, with larger modulation depths giving better F-values.

We found that using waveforms such as square, triangular, or saw-tooth for both excitation and gain gave poor F-values for harmonics higher than 1, as they have low

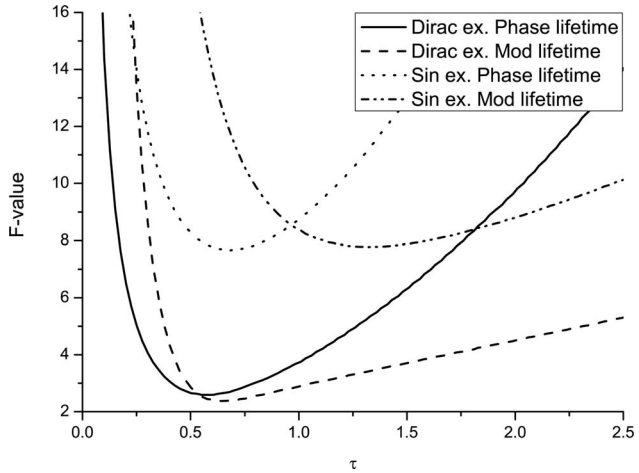

Fig. 5. Graph of the F-value as a function of τ for Dirac excitation and sinusoidal excitation with sinusoidal gain (modulation depth of 1.0) and three phase steps.

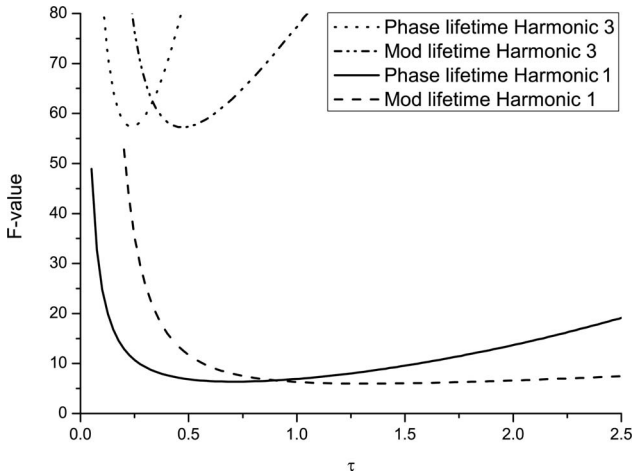

Fig. 6. Graph showing the F-value calculated from the first and third harmonics as a function of τ for square excitation with square gain for both phase and modulation lifetimes. The lifetime calculated from the third harmonic has a large F-value, indicating poor measurement quality.

excitation and gain modulation depths (1.27 versus 0.42 for the first and third harmonics, respectively, of a square wave). This is demonstrated in Fig. 6 for square wave excitation with square wave gain, where the third harmonic (the second nonzero harmonic for an odd square wave) has minimum F-values of 57 and 57 compared to the F-values from the first harmonic of 6.3 and 6.0 for the phase and modulation lifetimes, respectively. Since the square of the F-value is proportional to the number of photons required for a particular measurement accuracy, this means that approximately 90 times more photons would be required for the third harmonic measurement to have the same error as the first harmonic measurement. The F-values achieved for the first harmonic are better than those for the case of sinusoidal excitation and gain due to the fact that the modulation depth of the first harmonic component of a square wave is 1.27, compared to 1 for sinusoidal excitation.

For the case of Dirac excitation we found that lifetimes evaluated from higher harmonics could give reasonable F-values. This is seen in Fig. 7 for the case of a square gain waveform, where harmonics 1, 3, and 5 (the first three nonzero harmonics) all give minimum F-values below 20. This is a promising result, as the gain profile of an image intensifier is approximately a square wave [18].

D. Uneven Phase Step Positioning for Sinusoidal Excitation

When only single harmonic sinusoidal gain waveforms are used, reliable lifetime information can still be obtained with unevenly spaced phase steps, as aliasing is not a problem. We found that by careful placement of the phase steps, lower F-values could be obtained. Two different approaches were tried: first, placing a cluster of phase steps around the "crossing points" (the triangles in Fig. 8) and second, placing a cluster of points around the "peaks and troughs" (the circles in Fig. 8).

We found that when points are clustered around the "crossing points," the F-value for the phase lifetime was lowered compared to evenly distributed phase steps and

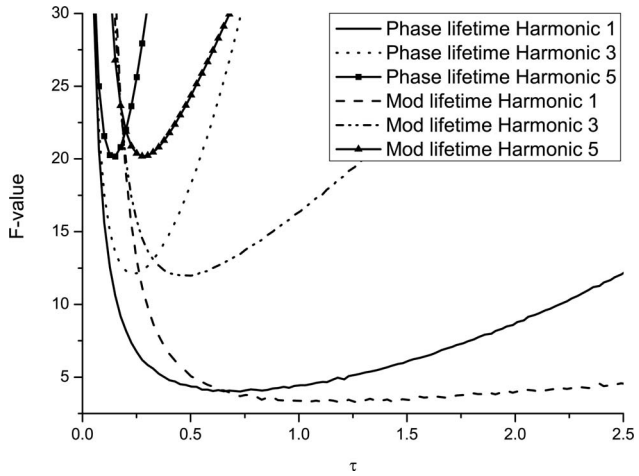

Fig. 7. Graph showing the F-value as a function of τ for Dirac excitation with square gain for phase and modulation lifetimes. The F-value data from higher harmonics are much better than for the case with square excitation.

the F-value for the modulation lifetime was raised. The opposite was true for points clustered around the "peaks and troughs." This was true for sinusoidal, square, and Dirac excitation. Figure 9 shows the phase and modulation lifetime F-values for Dirac excitation and sinusoidal gain with uneven phase steps. Twelve phase steps were used, clustered around the "crossing points" for phase and around the "peaks and troughs" for modulation lifetime measurements, with varying amounts of spread between the individual steps (5° or 10°; note that 30° with 12 phase steps corresponds to evenly spaced phase steps).

This analysis shows an optimum phase and modulation F-value of 2.9 and 2.0, respectively. This optimum occurred at modulation frequencies of $\tau=0.68$ and $\tau=0.65$ for the 5° phase step spacing and is over a 25% improvement compared to the evenly spaced phase step case. An analysis with sinusoidal excitation showed a similar improvement in the optimum phase and modulation F-values to 6.4 and 7.1, respectively. The disadvantages of this approach are that an approximate lifetime must be known roughly *a priori*, as otherwise the "peaks and troughs" and "crossing points" cannot be located, and that

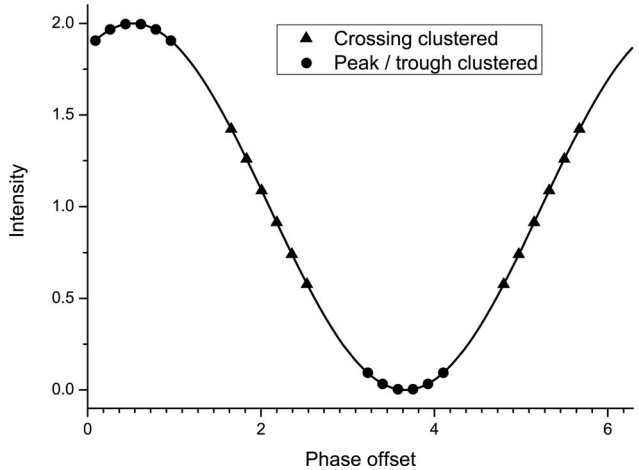

Fig. 8. Diagram explaining the location of "crossing points" and "peaks and troughs" for uneven phase step positioning.

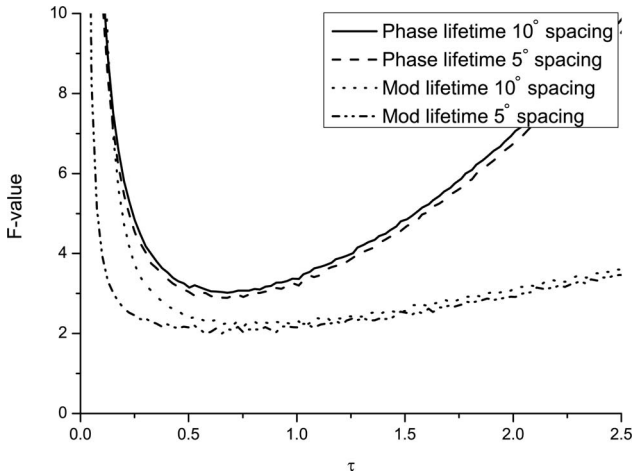

Fig. 9. Graph showing the phase F-value as a function of τ for Dirac excitation with sinusoidal gain (modulation depths of 1.0). The phase steps were clustered around the "crossing points" or "peaks and troughs" of the detected signal, with spreads of 5° and 10° shown for both phase and modulation lifetimes.

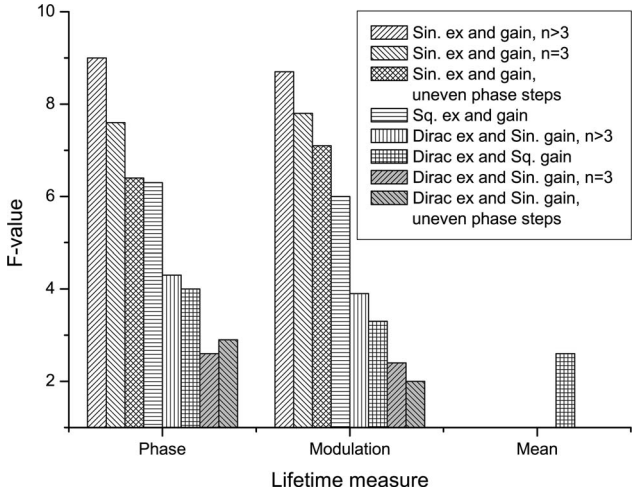

Fig. 10. Comparison of the optimum F-values calculated for different operating parameters.

the gain or excitation waveform must not contain multiple harmonics (otherwise aliasing may lead to artifacts in the lifetime analysis). Decreasing the separation of phase steps too far results in a very narrow range of τ in which good F-values are found for a given set of phase step locations. This is undesirable, as in reality an image will have a lifetime variation in it, and this is often precisely what one aims to measure. Further investigation is required to fully develop the potential of using uneven phase steps to obtain less noisy measurements.

All of these results are summarized in Fig. 10.

11. CONCLUSIONS

In conclusion, we have developed a theoretical framework, backed up by Monte Carlo simulations, which allows calculation of F-values for FD-FLIM with arbitrary excitation and gain profiles. The analysis is more rigorous than previous work, as it takes into account the data fitting procedure used in actual experiments and allows for

the arbitrary choice of excitation and gain waveforms. Using the theoretical framework developed, we found F-values that were significantly different from previously reported work and which changed markedly between different imaging scenarios. Since measurement accuracy and collection time are very important parameters for choosing between different lifetime imaging techniques, this is an important result. Previous work had shown FD-FLIM to have F-values higher than competing techniques, such as time-gated imaging, but this work shows that with the correct setup the F-values achievable can approach similar values. For example, a typical time-gated system with two gates has an optimum F-value of 1.7, compared to the optimal case shown here of 2.0 for Dirac excitation with sinusoidal gain and uneven phase steps. Also, previous work showed optimal F-values for Dirac excitation occurred as $\tau \rightarrow 0$, which in real experiments is not accessible. In the results shown here, optimal F-values occur in the range $\tau = 0.5 \rightarrow 1.5$, which for a typical lifetime of 3.0 ns corresponds to a range of 26 $\rightarrow$80 MHz modulation frequency. This is readily achieved with current technologies [7,19]. Additionally, F-values for time-domain techniques are for parallel acquisition. New technologies allowing parallel acquisition for FD-FLIM data [14] will increase the photon efficiency further.

The markedly different F-values obtained for different imaging scenarios shows the importance of system optimization in order to achieve the best possible sensitivity. Generally, we found that the best F-values are obtained by having a high modulation depth on both the excitation and gain waveforms. As such, Dirac pulse excitation gave by far the best F-values. The best gain waveform tested for even phase steps was a square wave; however, ongoing work is investigating the effect of rectangular gain profiles with reduced duty cycles. If a pure sinusoid is used as either the gain or excitation profile, then better F-values can be found by using only three phase steps. However, F-values can be further improved by using $N \geqslant 4$ along with careful positioning of the phase step locations. In addition we showed that when both gain and excitation waveforms contain higher harmonics, a lifetime and associated F-value could be calculated for each higher harmonic present. For multiharmonic sinusoidal (e.g., square wave) excitation, we found that the F-values for higher harmonics were extremely high, indicating very noisy measurements. However, for Dirac excitation the F-values for higher harmonics were more reasonable. This suggests that for multiple frequency FLIM measurements [18] a Dirac pulse would be a much better choice of excitation waveform than, say, a square wave. Interestingly, we found that adding extra phase steps did not reduce the F-value as might be expected. This means extra phase steps can be used to combat the problem of aliasing without reducing the photon economy.

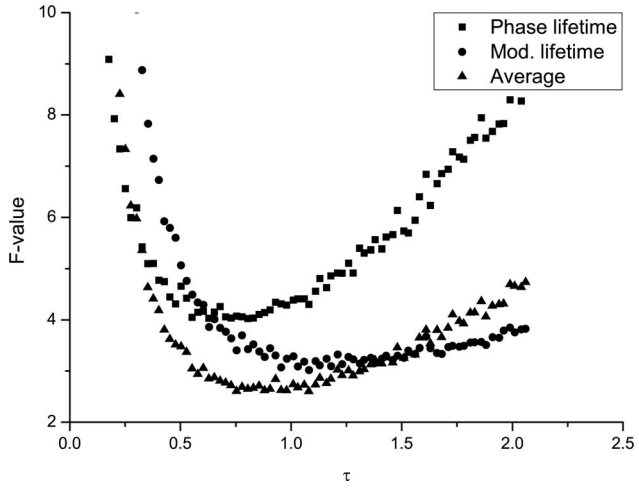

Fig. 11. Graph showing how the mean of phase and modulation lifetimes can produce a lifetime measurement with an F-value better than that for either measurement alone. This is because the two measurements are taken in parallel. The case shown is Dirac excitation with square gain (compare to Fig. 7).

It should be noted that phase and modulation lifetimes from all harmonics are acquired in parallel. Initial investigations show that performing a weighted fitting to all these data sets simultaneously can give even better F-values over a larger range of values of τ, although this calculation is limited to Monte Carlo experiments because of its complexity. Figure 11 shows the Monte Carlo calculation for Dirac excitation with square gain, where the F-value of the mean lifetime, $\tau_{mean} = 0.5(\tau_p + \tau_m)$, is calculated. In this case the mean lifetime shows a better F-value over a large range of values of τ.

ACKNOWLEDGMENTS

This work was supported by grants from the Engineering and Physical Sciences Research Council (EPSRC). C. F. Kaminski is grateful to the Leverhulme Trust for personal sponsorship.

REFERENCES

1. J. R. Lakowicz, H. Szmacinski, K. Nowaczyk, K. W. Berndt, and M. Johnson, "Fluorescence lifetime imaging," Anal. Biochem. **202**, 316–330 (1992).
2. K. Suhling, "Fluorescence lifetime imgaging," in *Methods Express, Cell Imaging*, D. Stephens, ed. (Scion, 2006), pp. 219–245.
3. W. Becker, A. Bergmann, M. A. Hink, K. König, K. Benndorf, and C. Biskup, "Fluorescence lifetime imaging by time-correlated single-photon counting," Microsc. Res. Tech. **63**, 58–66 (2004).
4. W. Becker, H. Hickl, C. Zander, K. H. Drexhage, M. Sauer, S. Siebert, and J. Wolfrum, "Time-resolved detection and identification of single analyte molecules in microcapillaries by time-correlated single-photon counting (TCSPC)," Rev. Sci. Instrum. **70**, 1835–1841 (1999).
5. K. Dowling, S. C. W. Hyde, J. C. Dainty, P. M. W. French, and J. D. Hares, "2-D fluorescence lifetime imaging using a time-gated image intensifier," Opt. Commun. **135**, 27–31 (1997).
6. A. D. Elder, J. H. Frank, J. Swartling, X. Dai, and C. F. Kaminski, "Calibration of a wide-field frequency-domain fluorescence lifetime microscopy system using light emitting diodes as light sources," J. Microsc. **224**, 166–180 (2006).
7. Q. S. Hanley, V. Subramaniam, D. J. Arndt-Jovin, and T. M. Jovin, "Fluorescence lifetime imaging: multi-point calibration, minimum resolvable differences, and artifact suppression," Cytometry **43**, 248–260 (2001).
8. A. Draaijer, R. Sanders, and H. C. Gerritsen, "Fluorescence lifetime imaging, a new tool in confocal microscopy," in *Handbook of Biological Confocal Microscopy*, J. Pawley, ed. (Plenum, 1995), pp. 491–505.
9. C. J. de Grauw and H. C. Gerritsen, "Multiple time-gate

module for fluorescence lifetime imaging," Appl. Spectrosc. **55**, 670–678 (2001).
10. R. M. Ballew and J. N. Demas, "An error analysis of the rapid lifetime determination method for the evaluation of single exponential decays," Anal. Chem. **61**, 30–33 (1989).
11. M. Kölner and J. Wolfrum, "How many photons are necessary for fluorescence lifetime measurements?" Chem. Phys. Lett. **200**, 199–204 (1992).
12. J. Philip and K. Carlsson, "Theoretical investigation of the signal-to-noise ratio in fluorescence lifetime imaging," J. Opt. Soc. Am. **20**, 368–379 (2003).
13. K. Carlsson and J. Philip, "Theoretical investigation of the signal-to-noise ratio for different fluorescence lifetime imaging techniques," Proc. SPIE **4622**, 70–78 (2002).
14. A. Esposito, T. Oggierc, H. C. Gerritsen, F. Lustenberger, and F. S. Wouters, "All-solid-state lock-in imaging for wide-field fluorescence lifetime sensing," Opt. Express **13**, 9812–9821 (2005).
15. P. C. Schneider, and R. M. Clegg, "Rapid acquisition, analysis, and display of fuorescence lifetime-resolved images for real-time applications," Rev. Sci. Instrum. **68**, 4107–4119 (1997).
16. F. R. Boddeke, "Quantitative fluorescence microscopy," Ph.D. dissertation (Technische Universiteit Delft, 1998).
17. K. Beers, *Numerical Methods for Chemical Engineering: Applications in MAT-LAB* (Cambridge U. Press, 2006).
18. A. Squire, P. J. Verveer, and P. I. H. Bastiaens, "Multiple frequency fluorescence lifetime imaging microscopy," J. Microsc. **197**, 136–149 (2000).
19. A. D. Elder, S. M. Matthews, J. Swartling, K. Yunus, J. H. Frank, C. M. Brennan, A. C. Fisher, and C. F. Kaminski, "Application of frequency-domain fluorescence lifetime imaging microscopy as a quantitative analytical tool for microfluidic devices," Opt. Express **14**, 5456–5467 (2006).